Clean Techn Environ Policy (2015) 17:1457–1473
DOI 10.1007/s10098-014-0870-0

ORIGINAL PAPER

Energy, economic, and environmental analysis of a flat-plate solar collector operated with SiO_2 nanofluid

M. Faizal · R. Saidur · S. Mekhilef · A. Hepbasli · I. M. Mahbubul

Received: 31 March 2014 / Accepted: 21 October 2014 / Published online: 5 November 2014

Abstract To overcome the environmental impact and declining source of fossil fuels, renewable energy sources need to meet the increasing demand of energy. Solar thermal energy is clean and infinite, suitable to be a good replacement for fossil fuel. However, the current solar technology is still expensive and low in efficiency. One of the effective ways of increasing the efficiency of solar collector is to utilize high thermal conductivity fluid known as nanofluid. This research analyzes the impact on the performance, fluid flow, heat transfer, economic, and environment of a flat-plate solar thermal collector by using silicon dioxide nanofluid as absorbing medium. The analysis is based on different volume flow rates and varying nanoparticles volume fractions. The study has indicated that nanofluids containing small amount of nanoparticles have higher heat transfer coefficient and also higher energy and exergy efficiency than base fluids. The measured viscosity of nanofluids is higher than water but it gives negligible effect on pressure drop and pumping power. Using SiO_2 nanofluid in solar collector could also save 280 MJ more embodied energy, offsetting 170 kg less CO_2 emissions and having a faster payback period of 0.12 years compared to conventional water-based solar collectors.

Keywords SiO_2 nanofluid · Flat-plate solar collector · Heat transfer · Economic · Exergy

M. Faizal
Department of Engineering, School of Liberal Arts and Sciences, Taylor's University Lakeside Campus, 47500 Selangor, Malaysia

M. Faizal · R. Saidur (✉) · I. M. Mahbubul
Department of Mechanical Engineering, Faculty of Engineering, University of Malaya, 50603 Kuala Lumpur, Malaysia
e-mail: saidur@um.edu.my; saidur912@yahoo.com

S. Mekhilef
Power Electronics and Renewable Energy Research Laboratory (PEARL), Department of Electrical Engineering, Faculty of Engineering, University of Malaya, 50603 Kuala Lumpur, Malaysia

A. Hepbasli
Department of Energy Systems Engineering, Faculty of Engineering, Yasar University, 35100 Izmir, Turkey

Introduction

Renewable energies are very important in the world economy today because they are sustainable, safe, and clean. World energy demand is increasing and expected to accelerate more in the future, while the fossil oil sources and production are declining. Climate change and environmental pollution are becoming huge global problems. Solar energy is an unlimited and free source of energy that can meet the world's future energy needs without harming the earth. Therefore, many studies have been conducted to address this issue. Tora and El-Halwagi (2009) had developed an optimal design of energy system to integrate solar systems and fossil fuel for sustainable and stable power outlet. Nemet et al. (2012) continued the work further by developing captured solar energy curve and minimal capture temperature curve to maximize the solar thermal energy delivered to the process. Ranjan and Kaushik (2013) performed an energy and exergy analysis of active solar distillation system integrated with solar pond that can contribute to water security and sustainability. Sanchez-Bautista et al. (2014) presented an optimization model for the optimal design of water-heating system for homes in Mexico. In that model, location, solar radiation, inhabitants, and time-based consumption pattern

were accounted to determine the optimal design of integrated solar, and boilers water-heating systems aimed to minimized cost and greenhouse gas emissions. There is a good potential for solar thermal energy in Malaysia due to its location on the equatorial, with hot and humid climate throughout the year and monthly solar radiation approximately around 400–600 MJ/m^2 (Mekhilef et al. 2012). However, the major problem for current solar heater is that the efficiency is low, and the price is ten times more expensive than electric heater. One of the effective methods to increase the efficiency of solar collector is to replace the working fluid with nanofluids.

Nanofluids were first introduced by Choi (1995), which are nanoparticles additives in liquid solvents. Researches on enhanced thermal efficiency of solar collector by applying nanofluids have been made in the past few years by the researchers. An experimental investigation conducted by Yousefi et al. (2012c) on the effect of Al_2O_3-based nanofluid shown an efficiency increase of 28.3 % of flat-plate solar collectors. Lenert and Wang (2012) presented a model and performed an experimental study of concentrated solar power application using carbon-coated cobalt (C-Co) nanoparticles and Therminol VP-1-based fluid. They concluded that the efficiency was more than 35 % with nanofluid, and the efficiency would increase with the increasing of nanofluid height. Lu et al. (2011) showed that the application of copper oxide (CuO) nanoparticles in evacuated tube solar collectors has significantly enhanced the thermal performance of evaporator which resulted in 30 % evaporating heat transfer coefficient increase compared to water as working fluid. 5 % improvement in the efficiency was found out by Otanicar et al. (2010) using variety of nanoparticles with water as base fluid for micro-solar-thermal collector. Shin and Banerjee (2011) applied novel nanomaterials in molten salts base fluid to concentrated solar power coupled with thermal storage and experienced an enhancement in operational efficiencies. Taylor et al. (2011) used graphite-based nanofluids in high flux solar collectors that resulted in 10 % increase in the efficiency. Zamzamian et al. (2014) performed an experimental study to investigate the effect of copper (Cu) nanoparticle on the efficiency of a flat-plate solar collector in different volume flow rates and weight fractions of the nanoparticles. It was found that the optimum point for solar collector efficiency has been reached up to 0.3 wt% Cu nanofluid at 1.5 L/min.

Smaller and more compact design of solar collector has become possible because of higher thermal conductivity of nanofluids. Because of higher thermal conductivity and efficiency of nanofluids, smaller and compact design of solar thermal collectors has become possible without affecting the output desired. Smaller size collector can reduce the material usage, cost, and energy required in manufacturing (Leong et al. 2012). Some studies were made on the potential of size reduction of various engineering applications using nanofluids. These were based on vehicle's weight reduction (Saidur and Lai 2011), building heat exchanger's heat transfer area (Kulkarni et al. 2009), reduction of air frontal area of a car radiator (Leong et al. 2010), and the size reduction of shell and tube recovery exchanger (Leong et al. 2012). Other studies had also been made to evaluate the economic and environmental impact of solar hot water system (Kalogirou 2004, 2008; Tsilingiridis et al. 2004; Ardente et al. 2005). One particular study focused on the environmental and economic analysis of direct absorption micro-solar thermal collector utilizing graphite nanofluid (Otanicar 2009). Studies on the potential of size reduction of flat-plate solar collectors has also been reported for multi-walled carbon nanotubes nanofluid (Faizal et al. 2013b) and Al_2O_3 nanofluid (Faizal et al. 2014).

Table 1 Properties of different nanomaterials and base fluids (Kamyar et al. 2012; Namburu et al. 2007)

Materials	Specific heat, C_p (J/kg K)	Thermal conductivity, k (W/m K)	Density, ρ (kg/m^3)
Alumina (Al_2O_3)	773	40	3,960
Copper oxide (CuO)	551	33	6,000
Titanium oxide (TiO_2)	692	8.4	4,230
Silicon dioxide (SiO_2)	765	36	2,330
Water (H_2O), base fluid	4,182	0.60	1,000

In thermodynamics analysis, the energy equation alone is insufficient to evaluate the flat-plate solar collector efficiency. The second law or exergy analysis is more effective to determine the source and magnitude of irreversibility, and can be used to improve the efficiency of the system. Exergy is the maximum output that can be achieved relative to the environment temperature (Cengel and Boles 2010). Studies on exergy analysis have been conducted by Saidur et al. (2012) on various solar energy applications and (Farahat et al. 2009) flat-plate solar collectors. Mahian et al. (2013) also comprehensively reviewed the entropy generation in nanofluids flow, while Alim et al. (2013) made an analytical analysis of entropy generation in a flat-plate solar collector using different types of metal oxide nanofluids. However, to the best of the authors' knowledge, experimental studies on solar collectors performance analysis using SiO_2 nanofluid have not yet appeared in the open literature even though a lot of

simulation works have been done, and all the studies on the exergy analysis on flat-plate solar thermal collectors are either simulation or theoretical. Therefore, this study focuses on the thermodynamics performance, heat transfer characteristic, economic, and environmental assessment of flat-plate solar collectors applying SiO_2 nanofluid to fill up those gaps.

Properties of nanofluids

By considering the application of nanofluids as the base of the research, various researchers have published research outcomes on the properties of nanoparticles and thermal properties of nanofluids. Table 1 shows the published specific heat, thermal conductivity, and density of different nanoparticles.

However, all these special characteristics cannot be achieved unless the nanoparticles are properly dispersed and stable.

Preparation and characterization of nanofluid

Stability of nanofluids for long term is the major issue for the engineering applications (Liu and Liao 2008). Nanoparticles in the base fluid naturally will aggregate and sediment. In theory, there is existence of both attractive and repulsive forces between particles (Ise and Sogami 2005). The attractive force is the van der Waals force, and the repulsive force is the electrostatic repulsion when particles get too close together. If the repulsive force is stronger than the attractive force, nanoparticles in the base fluid can remain stable or otherwise it will aggregate and serious aggregation will lead to sedimentation. Adding surfactants to the nanofluid can enhance the electrostatic repulsion of nanoparticles. Surfactants such as sodium dodecyl benzene sulfonate, sodium dodecyl sulfate, or Triton X-100 had been tested and proven to stabilize nanofluid (Wang 2009). However, the effect might be affected when the Brownian motion of nanoparticles is too strong or when the nanofluid is heated. Another way to stabilize nanofluid is by changing the pH value of the solution (Yousefi et al. 2012a). The pH of isoelectric point for nanoparticles carries no electrical charge and, therefore, causes no interparticle repulsion force which in turn causing more aggregated solution. The more differences between the pH of nanofluid and pH of isoelectric point may cause less aggregation and better dispersion. The pH of SiO_2 in this study had been measured to be 6.5 using Hanna Instruments microprocessor pH meter, while the pH of isoelectric point for SiO_2 is around 3 (Kosmulski 2001). A better way to stabilize nanofluid was proposed by Yang and Liu (2010) who is to graft polymers

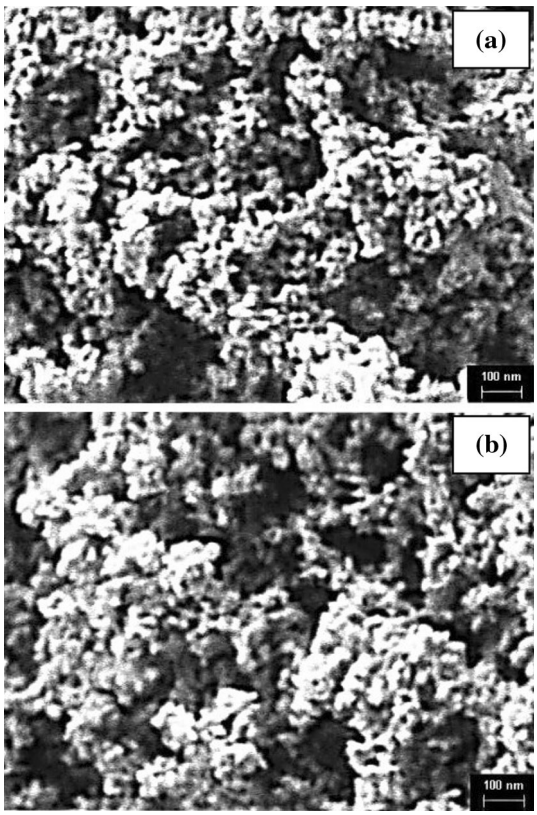

Fig. 1 SEM images of SiO_2 nanoparticle **a** before and **b** after the experiment

on to the surface of nanoparticles and also known as surface functionalization. Silanes were grafted on silica nanoparticles making "Si-O-Si" covalent bonding and resulting in steric stabilization effect even when heated. Functionalized SiO_2 nanoparticles have been reported to keep dispersing well after 12 months, and no sedimentation was observed (Chen et al. 2013).

The SiO_2 nanoparticles used in the experiments were obtained from US Research Nanomaterials, Inc. with 15 nm in outer diameter, coated with 2 wt% silane, which have a density of 2.4 g/cm^3 and a pH value of 6–6.5. For this study, 3 L of 0.2 and 0.4 % volume fraction of SiO_2 nanofluid were prepared. The amount of nanoparticles needed for the intended volume fraction of the solution was calculated first from

$$\phi_n = \frac{m_n/\rho_n}{m_n/\rho_n + m_w/\rho_w}, \quad (1)$$

where ϕ_n is the volume fraction of nanoparticles in nanofluid (%), m_n is the mass of nanoparticle (kg), m_w is the mass of water (kg), ρ_n is the density of nanoparticle (kg/m^3), and ρ_w is the density of water (kg/m^3).

The nanofluids were prepared using two-step method. It was prepared by dispersing nanoparticles into distilled

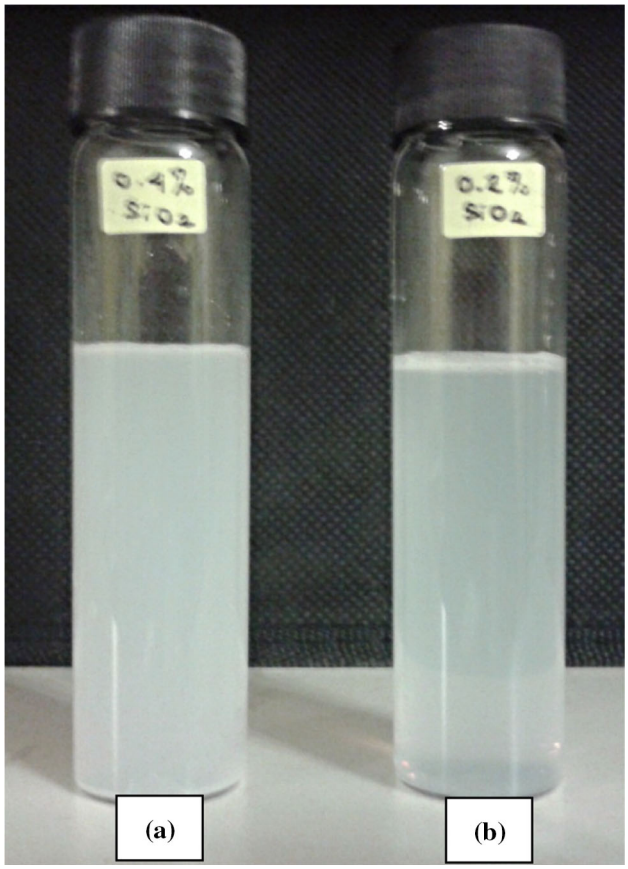

Fig. 2 Pictures of **a** 0.4 % and **b** 0.2 % nanofluid after 6 months

water using ultrasonicator and high pressure homogenizer (up to 2,000 bar capacity) to obtain a homogenously dispersed solution. The microstructure and composition of the nanoparticles are characterized using field emission scanning electron microscopy (FESEM; Model AURIGA, Zeiss, Germany). Nanoparticles are characterized before and after experiment with FESEM at 1 kV accelerating voltage. 50,000 times magnification is used to capture the images at the 100 nm scale. Figure 1 shows the FESEM images of SiO_2 nanoparticles mixed in distilled water. The picture of the prepared nanofluid is shown in Fig. 2. As it is shown, the prepared nanofluid can still keep dispersing well after 6 months, and no sedimentation was observed.

The viscosity of prepared nanofluid was measured using LVD-III ultra-programmable rheometer (Brookfield, USA) with ±0.5 % uncertainty. The viscosity of all samples was measured at the constant shear rate of 73.38 s^{-1}, while the ULA spindle rotating was 60 rpm. For the temperature variation, the refrigerated circulator bath (Model AD07R-40-12E, Polyscience, USA) with accuracy ±0.1 °C was connected to the water jacket of ULA that was attached to the rheometer. The temperature of each sample was varied from 25 to 85 °C with 20 °C intervals to investigate the

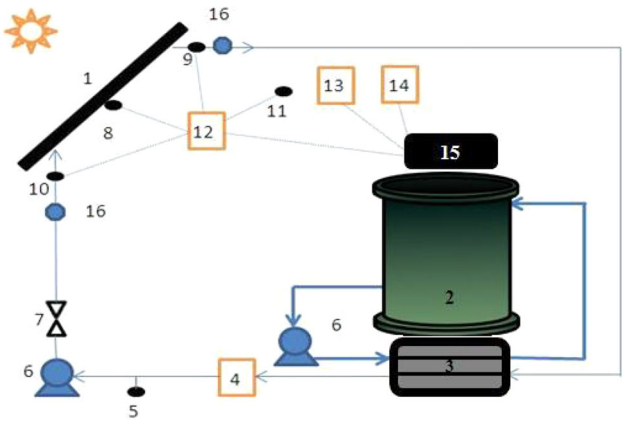

Fig. 3 A schematic diagram of the experiment: *1* flat-plate solar collector, *2* water tank, *3* heat exchanger, *4* flow meter, *5* drain, *6* pump, *7* valve, *8* thermocouple (plate temperature), *9* thermocouple (working fluid out), *10* thermocouple (working fluid in), *11* thermocouple (ambient), *12* thermometer, *13* TES 1333R solar meter, *14* PROVA (AV M-07) anemometer, *15* data logger, *16* pressure transducer

effect of temperature on the viscosity of nanofluid. Each experiment was repeated three times to get the more precise values. The mean value of the three data was considered for the analysis.

Experimental procedure

A schematic diagram of the experiment is shown in Fig. 3. The solar collector experimental setup indicated in Fig. 4 was constructed at the University of Malaya, Kuala Lumpur, Malaysia. The specifications of the flat-plate solar collector used in this study are given in Table 2. The tilt angle of this solar collector is 22°. Two electrical pumps were used in this system to pump the working fluid and water from the tank. The water from the tank is used to absorb the heat from the system cycle. A plate heat exchanger is used to transfer the heat from the working fluid of the solar thermal system cycle to the water inside the tank. The experiments were conducted using different volume flow rates from 1 to 3 L/s for each type of the working fluids. A flow meter with a controlling valve was connected to control the mass flow rate of the working fluid. The tests have been carried out from 10 am to 3 pm. Following the requirement of the ASHRAE (2010) standard, each test was performed in several days, and the best experimental data were chosen. For steady-state efficiency tests, the mass flow rate must be held within ±1 %, solar radiation must be steady within ±50 W/m^2, the variation of environment temperature must not more than ±1.5 K, and the inlet temperature must be within ±0.1 K. Steady-state conditions must be maintained for data period length of

Fig. 4 Experimental setup

Table 2 Solar collector's specification

Specification	Dimension
Dimension	2,000 mm × 1,000 mm × 80 mm ($L \times W \times T$)
Aperture area	1.84 m^2
Weight	36 kg
Cover material	4 mm tempered texture glass
Heat transfer coefficient	4.398 W/(m^2 K)
Absorber material	0.4 mm aluminum
Header material	Copper TP2
Header tube size	22 mm × 0.6 mm (Φxt), 2 pcs
Riser tube material	Copper TP2
Riser tube size	10 mm × 0.45 mm (Φxt), 8 pcs
Absorption rate	0.94
Emittance	0.12
Frame	Aluminum alloy, anodized

5 min and pre-data period of 15 min. Thermocouples were used in this experiment to measure the plate temperature, the fluid temperatures at the inlet and outlet of the solar collector, and the environment temperature. A pressure transducer was used to measure the pressure difference from the inlet and outlet of the solar collector. All readings from the thermocouples and the pressure transducer were recorded in the data logger. Solar radiation was recorded using a TES 1333R solar meter. The wind speed was measured by an anemometer. The entire measuring devices had been carefully calibrated before, during, and after the experiment.

Analyses

Error analysis

In any experiment, the measured quantities subject to uncertainties or error. Errors can be caused by various factors. The errors can be classified as systematic and random error. Systematics errors are errors that shifted or displaced the measurement values systematically such as incorrect calibration of equipment or incorrect adjustment of that device. Usually, systematic errors can be avoided and eliminated. Random errors, on the other hand, are errors which fluctuate from one measurement to the next. Random errors are unavoidable and must be accounted to indicate the accuracy of the measured data (Kotulski and Szczepinski 2010).

For a collection of measured data, it is very important to calculate the average or mean value $\bar{x}$. The mean value can be calculated as follows:

$$\bar{x} = \frac{\sum x_i}{n}, \tag{2}$$

where n is the number of times and x_i is the measured quantity.

$\bar{x}$ The measurement of dispersion in the data collection relative to its average value is an important parameter in error analysis. The variance s^2 is the usual measure for estimating distribution dispersion. Variance is the arithmetical mean value of all squares of deviations of particular values x_i from the average values of the entire samples and can be defined by the following formula (Kotulski and Szczepinski 2010):

$$s^2 = \frac{\sum (x_i - \bar{x})^2}{n-1}. \tag{3}$$

The quantity s is called the standard deviation which determines the width of the distribution and can be calculated by

$$s = \sqrt{s^2}. \tag{4}$$

The uncertainty given by the manufacturer for all the measuring devices is ±2 % for PROVA (AV M-07) anemometer, ≤±0.06 °C for thermocouples, and ≤±2 % for flow meter. After the uncertainties of measured data have been accounted, the uncertainty for calculated results will also be quantified using Kline and McClintock method (1953).

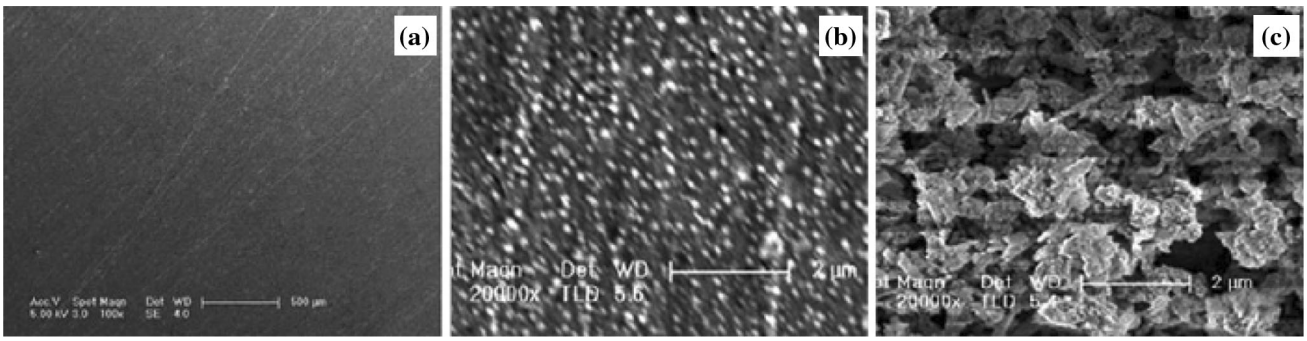

Fig. 5 SEM images of the heated surface of **a** before the experiment, **b** using the functionalized nanofluid, and **c** using the conventional nanofluid (Yang and Liu 2010)

Surface state of the heated surface

Nanoparticles had been reported to precipitate or fouled on the heated surface or on the flow conduit wall which will significantly change the surface characteristics that can potentially affect the thermal performance as well. Conventional SiO_2 nanofluid (without surface coating) formed a fouling layer of nanoparticles on the heated surface after the boiling experiment, and the fouling layer cannot be flushed away by water. However, for SiO_2 nanoparticles coated with silane, no fouling layer exists after the boiling process. The SEM images of heated surface are shown in Fig. 5. As seen in Fig. 5, only scattered functionalized nanoparticles are observed on the heated surface which can be easily flushed away by water. Similar result was also shown by Chen et al. (2013) indicating that no deposition layer exists for functionalized nanofluid. The test had been repeated using distilled water again after nanofluid experiment to check if the nanoparticle precipitation on the flow conduits will significantly change the surface characteristics that can potentially affect the thermal performance of the solar collector. From the test, the results shown that there is no significant impact of using functionalized nanofluid on surface characteristics of solar collector. The results obtained using distilled water after nanofluid experiment were similar with the one before nanofluid had been applied in the solar collector.

Efficiency analysis of nanofluid-based flat-plate solar collector

The collector thermal efficiency can be calculated from the ratio of the useful energy to the energy incident on the collector. Flat-plate collectors can collect both direct and diffuse solar radiation. To predict and model the collector performance, information on the solar energy absorbed by the collector absorber plate is needed. The solar energy incident radiation on a tilted surface consists of beam, diffuse, and ground-reflected radiation (Kalogirou 2009).

The beam and diffuse solar radiation will travel through the transparent cover. Increase in transmittance (τ) of the glazing of solar collector will result in more radiation received by the absorber plate. The energy will be absorbed in a fraction equal to the absorptivity (α) of the black absorber plate. Absorptivity would be one for the perfect blackbody absorber. The instantaneous energy gained by the receiver can be determined by Foster et al. (2009)

$$\dot{Q}_{\mathrm{r}} = \dot{q}_{\mathrm{r}} A_{\mathrm{p}} = (\tau\alpha)_{\mathrm{eff}} I_{\mathrm{T}} A_{\mathrm{p}}, \tag{5}$$

where $(\tau\alpha)_{\mathrm{eff}}$ is the effective optical fraction of the energy absorbed, τ is the transmissibility of the transparent cover, α is the absorptivity of the absorber, A_{p} is the collector aperture area (the frontal opening area of the collector), and I_{T} is the solar radiation incident on the tilted collector. I_{T} is the sum of component of beam radiation I_{b}, sky diffuse radiation I_{d}, and ground-reflected solar radiation I_{r}, and can be expressed as

$$I_{\mathrm{T}} = I_{\mathrm{b}} + I_{\mathrm{d}} + I_{\mathrm{r}}. \tag{6}$$

The radiation will be absorbed and heat the absorber plate. Generally, solar collectors have great heat losses. The purpose of glazing is to prevent infrared thermal energy to escape. However, the temperature difference between the absorber plate and the ambient causes heat losses by convection to the surroundings. This heat loss can be calculated by Foster et al. (2009)

$$\dot{Q}_{\mathrm{conv}} = \dot{q}_{\mathrm{conv}} A_{\mathrm{p}} = U A_{\mathrm{p}} \left(T_{\mathrm{p}} - T_{\mathrm{a}}\right), \tag{7}$$

where U is the overall heat loss coefficient, T_{P} is absorber's plate temperature, and T_{a} is the ambient temperature.

The heat lost rate by radiation can be calculated by Foster et al. (2009)

$$\dot{Q}_{\mathrm{rad}} = \dot{q}_{\mathrm{rad}} A_{\mathrm{p}} = \varepsilon_{\mathrm{eff}} \sigma A_{\mathrm{p}} \left(T_P^4 - T_a^4\right), \tag{8}$$

where $\varepsilon_{\mathrm{eff}}$ is the effective emissivity of the collector and σ is Stefan–Boltzmann constant.

The heat losses from the bottom and from the edges of the collector are very small due to the insulation and can be

neglected. Combining Eqs. (8) and (9) above, the useful energy collected can be represented as

$$\dot{Q}_u = \dot{q}_u A_p = (\tau\alpha)_{eff} I_T A_p - U A_p (T_p - T_a) - \varepsilon_{eff} \sigma A_p \left(T_p^4 - T_a^4\right). \quad (9)$$

The heat-conducting fluid is the important of all for this analysis. The fluid will pass through pipes attached to the absorber plate. The fluid will absorb heat from the plate as it flows through the pipes and increased its temperature for useful application. The thermal efficiency of a solar collector can be calculated as

$$\eta = \frac{\dot{Q}_u}{I_T A_p}. \quad (10)$$

To relate the collector's actual performance directly and in terms of the temperature of the useful heat energy from the circulating fluid, the efficiency and the useful heat gain can be calculated from

$$\eta = F_R \left[(\tau\alpha)_{eff} - \frac{U A_p}{I_T A_p}(T_{in} - T_a)\right], \quad (11)$$

$$\dot{Q}_u = \eta I_T A_p = I_T A_p F_R \left[(\tau\alpha)_{eff} - \frac{U A_p}{I_T A_p}(T_{in} - T_a)\right], \quad (12)$$

where F_R is the effectiveness removal factor and T_{in} is the fluid inlet temperature.

The important useful heat gain by the working fluid can be expressed as

$$\dot{Q}_u = \dot{m} C_p (T_{out} - T_{in}), \quad (13)$$

where T_{out} is the fluid outlet temperature, C_p is the heat capacity at constant pressure, and $\dot{m}$ is the mass flow rate of the working fluid.

The heat capacity of nanofluid can be calculated by Zhou and Ni (2008)

$$C_{p,nf} = C_{p,np}(\varphi_n) + C_{p,bf}(1 - \varphi_n), \quad (14)$$

where $C_{p,nf}$ is the heat capacity of nanofluid, $C_{p,np}$ is the heat capacity of nanoparticles, $C_{p,bf}$ is the heat capacity of base fluid, and φ_n is the volume fraction of nanoparticles in nanofluid.

When there is no fluid flow, the temperature of the absorber can be defined as stagnation temperature (Singal 2008):

$$T_{stag} = T_a + \frac{I_T F_R (\tau\alpha)_{eff}}{(F_R U) R}. \quad (15)$$

From all these expressions, the useful heat gain and the efficiency of collectors can be calculated and compared between the conventional working fluid and SiO_2 nanofluids.

Exergy analysis of nanofluid-based flat-plate solar collector

Exergy is the maximum output that can be achieved relative to the environment temperature. The general equation of the exergy balance is (Farahat et al. 2009; Suzuki 1988)

$$\dot{E}_{in} + \dot{E}_s + \dot{E}_{out} + \dot{E}_l + \dot{E}_d = 0, \quad (16)$$

where $\dot{E}_{in}$ is the inlet exergy rate, $\dot{E}_s$ is the stored exergy rate, $\dot{E}_{out}$ is the outlet exergy rate, $\dot{E}_l$ is the leakage exergy rate, and $\dot{E}_d$ is the destroyed exergy rate.

The inlet exergy rate measures the fluid flow and the absorbed solar radiation rate. The inlet exergy rate with fluid flow can be calculated by Farahat et al. (2009)

$$\dot{E}_{in,f} = \dot{m} C_p \left(T_{in} - T_a - T_a \ln\left(\frac{T_{in}}{T_a}\right)\right) + \frac{\dot{m}\Delta P_{in}}{\rho}, \quad (17)$$

where ΔP_{in} is the pressure difference of the fluid with the surroundings at entrance and ρ is the fluid density.

The absorbed solar radiation exergy rate can be calculated as

$$\dot{E}_{in,Q} = \eta I_T A_p \left(1 - \frac{T_a}{T_s}\right), \quad (18)$$

where T_s is the apparent sun temperature and equals to 75 % of blackbody temperature of the sun (Bejan et al. 1981).

Total inlet exergy rate of the solar collector can be calculated from

$$\dot{E}_{in} = \dot{E}_{in,f} + \dot{E}_{in,Q}. \quad (19)$$

At steady-state conditions, where the fluid is flowing, the stored exergy rate is zero:

$$\dot{E}_s = 0. \quad (20)$$

When only the exergy rate of the outlet fluid flow is considered, the outlet exergy rate can be defined as (Kotas 1995)

$$\dot{E}_{out,f} = -\dot{m} C_p \left(T_{out} - T_a - T_a \ln\left(\frac{T_{out}}{T_a}\right)\right) + \frac{\dot{m}\Delta P_{out}}{\rho}. \quad (21)$$

The heat leakage from the absorber plate to the environment can be defined as the leakage exergy rate and calculated as (Gupta and Saha 1990)

$$\dot{E}_l = -U A_p (T_p - T_a)\left(1 - \frac{T_a}{T_p}\right). \quad (22)$$

The destroyed exergy rate caused by the temperature difference between the absorber plate surface and the sun can be expressed as (Gupta and Saha 1990)

$$\dot{E}_{d,\Delta T_s} = -\eta I_T A_p T_a \left(\frac{1}{T_p} - \frac{1}{T_s}\right). \quad (23)$$

The destroyed exergy rate by pressure drop is expressed by (Suzuki 1988)

$$\dot{E}_{d,\Delta P} = -\frac{\dot{m}\Delta P}{\rho} \frac{T_a \ln\left(\frac{T_{out}}{T_a}\right)}{(T_{out} - T_{in})}. \quad (24)$$

The destroyed exergy rate caused by the temperature difference between the absorber plate surface and the agent fluid can be calculated using the following relation (Suzuki 1988):

$$\dot{E}_{d,\Delta T_f} = -\dot{m}C_p T_a \left(\ln\left(\frac{T_{out}}{T_{in}}\right) - \frac{(T_{out} - T_{in})}{T_p}\right). \quad (25)$$

The total destroyed exergy rate can be calculated from

$$\dot{E}_d = \dot{E}_{d,\Delta T_s} + \dot{E}_{d,\Delta P} + \dot{E}_{d,\Delta T_f}. \quad (26)$$

The exergy destruction rate can also be expressed as

$$\dot{E}_d = T_a \dot{S}_{gen}, \quad (27)$$

where $\dot{S}_{gen}$ is the overall rate of entropy generation and can be calculated from (Bejan 1996)

$$\dot{S}_{gen} = \dot{m}C_p \ln\frac{T_{out}}{T_{in}} - \frac{\dot{Q}_S}{T_S} + \frac{\dot{Q}_O}{T_a}, \quad (28)$$

where $\dot{Q}_S$ is the solar energy rate absorbed (W) by the collector surface as expressed by (Esen 2008)

$$\dot{Q}_S = I_T(\tau\alpha)A_p, \quad (29)$$

and $\dot{Q}_O$ is the heat loss rate to the environment (W):

$$\dot{Q}_O = \dot{Q}_S - \dot{m}C_p(T_{out} - T_{in}). \quad (30)$$

Ultimately, combining all the expression above, the exergy efficiency equation of the solar collector can be given as follows (Farahat et al. 2009):

$$\eta_{ex} = \frac{\dot{m}\left[C_p\left(T_{out} - T_{in} - T_a \ln\left(\frac{T_{out}}{T_{in}}\right)\right) - \frac{\Delta P}{\rho}\right]}{I_T A_p\left(1 - \frac{T_a}{T_s}\right)}. \quad (31)$$

Pumping power

In this system, an electrical powered pump is required to pump the working fluid throughout the collector. To analyze the pumping energy needed by the system, the expressions from White (2003) and Garg and Agarwal (1995) were used. The pressure drop in the system can be calculated from

$$\Delta P = f\frac{\rho V^2}{2}\frac{\Delta L}{D} + K\frac{\rho V^2}{2}, \quad (32)$$

where f is the friction factor, K is the loss coefficient, and D is the diameter of the pipe. V is the velocity (m/s) of the working fluid and can be calculated from

$$V = \frac{\dot{m}}{\rho_{nf}\pi D^2/4}. \quad (33)$$

The density of nanofluid can be calculated from

$$\rho_{nf} = \rho_{np}(\varphi_n) + \rho_{bf}(1 - \varphi_n). \quad (34)$$

The friction factors for laminar flow ($Re \leq 2 \times 10^5$) and turbulent flow ($Re \leq 2 \times 10^5$) can be calculated from (35) and (36), respectively (Bergman et al. 2011; Kahani et al. 2013):

$$f = \frac{64}{Re}, \quad (35)$$

$$f = \frac{0.079}{(Re)^{1/4}}. \quad (36)$$

The Reynolds number can be expressed as

$$Re = \frac{\rho VD}{\mu}, \quad (37)$$

where μ is the viscosity of the working fluid (0.0008 kg/m s for water) and the viscosity of nanofluid was measured using LVD-III ultra-programmable rheometer (Brookfield, USA).

Finally, the pumping power can be obtained using

$$\dot{W}_{pumping} = \left(\frac{\dot{m}}{\rho_{nf}}\right) \times \Delta P. \quad (38)$$

Heat transfer

The convective heat transfer coefficient in this study can be calculated from

$$h = \frac{Q_u}{A_p(T_p - T_b)}, \quad (39)$$

where T_b is the bulk temperature and can be calculated from

$$T_b = \frac{T_{in} + T_{out}}{2}. \quad (40)$$

The heat transfer coefficient can also be obtained from Li et al. (2003)

$$h = \frac{q}{T_p - T_{nf}}, \quad (41)$$

where q is the heat flux (W/m^2).

From there, the Nusselt number can be calculated as

$$Nu_{\mathrm{nf}} = \frac{h_{\mathrm{nf}} D}{k_{\mathrm{nf}}}. \quad (42)$$

For the laminar flow of circular pipe, the Nusselt number can be calculated from the Reynolds and Prandtl numbers expressed by Owhaib and Palm (2004)

$$Nu = 0.000972 Re^{1.17} Pr^{1/3} \quad \text{for} \quad Re < 2,000. \quad (43)$$

Prandtl number can be calculated from

$$Pr = \frac{C_{\mathrm{p,nf}} \mu_{\mathrm{nf}}}{k_{\mathrm{nf}}}. \quad (44)$$

The thermal conductivity can be expressed by

$$\frac{k_{\mathrm{nf}}}{k_{\mathrm{f}}} = \frac{k_{\mathrm{p}} + (\mathrm{SH}-1)k_{\mathrm{f}} - (\mathrm{SH}-1)\varphi(k_{\mathrm{f}} - k_{\mathrm{p}})}{k_{\mathrm{p}} + (\mathrm{SH}-1)k_{\mathrm{f}} + \varphi(k_{\mathrm{f}} - k_{\mathrm{p}})}, \quad (45)$$

where SH is the shape factor and assuming the spherical shape of nanoparticle, the factor can be taken as 3 (Li et al. 2013).

Embodied energy analysis

After that, the embodied energy of a solar collector can be estimated. Only energy used to manufacture the solar collector is considered where else the distribution, maintenance, and disposal phases of the collectors are neglected. Due to more than 70 % of the embodied energy of the system come from the manufacturing of the collector (Ardante et al. 2005), the analysis was done with the reduction of the collector area as the functional unit that influences the overall weight and embodied energy of the collector. Using the thermal efficiency data of the solar collector, the potential of reduction of the size of collector's area can be estimated by

$$A_{\mathrm{p}} = \frac{\dot{m} C_{\mathrm{p}} (T_{\mathrm{out}} - T_{\mathrm{in}})}{I_{\mathrm{T}} \eta}. \quad (46)$$

Two major materials are used in the solar collector namely glass and copper with the weight ratio of 27 kg glass and 9 kg copper for a 36 kg collector. The embodied energy indices are 15.9 and 70.6 MJ/kg for the glass and the copper, respectively (Otanicar et al. 2010). Using the result of size reduction, weight and embodied energy for the solar collector can be calculated accordingly.

Economic analysis

The results of the thermal performance of nanofluid solar collector and size reduction can also be used to estimate the cost saving. Using nanofluid as working fluid in the solar collector, large portion of the copper and the glass used in the system can be eliminated based on the scaling of the overall percentage weight of the collector. The capital cost of the collector will then be offset by the cost of the nanoparticles. The energy usage per day in conjunction with the local electricity rates based on 0.07 USD/kWh for the first 200 kWh and 0.10 USD for the subsequent hour are used to determine the amount saved using a solar thermal system. Using a solar hot water system, 11.03 % of electricity used for water heating in Malaysia can be saved (Lalchand 2012).

Table 3 Electricity generation by fuel type and primary emissions mix for Malaysia (Sustainable Energy Development 2010)

Fuel	% of Electricity generated	Carbon dioxide, CO_2 (kg/MJ)	Sulfur oxides, SO_x (kg/MJ)	Nitrogen oxides, NO_x (kg/MJ)
Coal	36.5	0.274	0.00031	0.0005
Oil	0.2	0.220	0	0
Natural gas	55.9	0.113	0	0.00003
Hydro	5.6	0	0	0
Others	1.8	0	0	0

Environmental analysis

Burning of fossil fuels to generate the energy to heat water will result in harmful gas emissions. Switching to solar hot water system can reduce that problem. The distribution of electricity from various fuel types and the key pollutants generated in Malaysia is shown in Table 3.

With the data of the embodied energy index of the solar collector achieved from "Embodied energy analysis" section, the emissions from the manufacturing of the collectors can be determined. The offset damage costs can be calculated for the three main pollutants of CO_2, NO_x, and SO_x based on the damage cost factors (Spardo and Rabl 1999). These offset damage costs are not costs directly applicable to the collector owner.

Results and discussion

Error analysis

The distributions of the measured values of solar radiation, wind velocity, and temperatures are specified in Table 4. Standard deviation determines the width of the distribution. Errors are quoted in terms of the standard deviation. For measured solar radiation, the standard deviation was around 27.39 W/m^2 for the average value of 756.76 W/m^2. The standard deviations for measured plate temperature, inlet temperature, outlet temperature, and ambient temperature are 5.67, 0.34, 6.86, and 1.21 °C, respectively. The maximum uncertainty obtained by combining both

Table 4 Mean value, variance, and standard deviation of the measurements

	Solar radiation, I_T (W/m^2)	Plate temperature, T_P (°C)	Inlet temperature, T_{in} (°C)	Outlet temperature, T_{out} (°C)	Ambient temperature, T_a (°C)
Mean, $\bar{x}$	756.76	54.69	35.26	46.53	33.46
Variance, s^2	749.94	32.13	0.11	47.08	1.46
Standard deviation, s	27.39	5.67	0.34	6.86	1.21

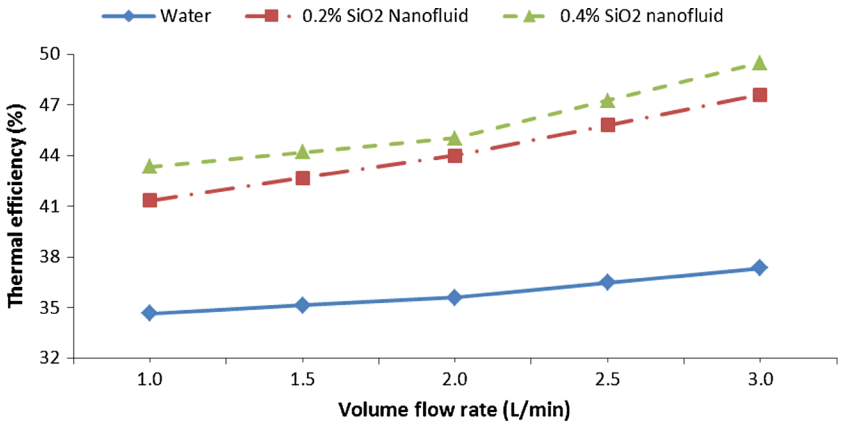

Fig. 6 Effect of volume flow rates of working fluids on the efficiency of the solar collector

measurement and random uncertainties at various tests was around 6.77 % in which the random uncertainty due to random fluctuation of the process contributes greater.

Efficiency analysis

The experimental results include the performance of solar collector using water and SiO_2 nanofluids at various concentrations and volume flow rates. The tests were performed around solar noon at 10 am to 3 pm. Figure 6 shows the effect of the volume flow rate of the working fluid on the efficiency of the solar collector. The volume flow rates of the working fluid were regulated to keep in between 1 and 3 L/min. For a steady-state condition in compliance with ASHRAE standard, the maximum variation in mass flow rate was kept at (<1 %). The uncertainty for collector efficiency calculation at various tests was around 4.1 % including both measurement and scatter uncertainties, and was quantified using Kline and McClintock method (1953).

As shown in Fig. 6, the efficiency of the solar collector with SiO_2 nanofluids is higher than that of the water, while the efficiency is increased by increasing the volume flow rates. There are some reasons for the higher efficiency of nanofluids solar collector compared to water. One of it is the higher output temperature associated with nanofluids solar collector (Yousefi et al. 2012a–c). The efficiency of solar collector increased by 23.5 % using 0.2 % SiO_2 nanofluid. However, only an increase of around 3.7 % was achieved by adding the concentration to 0.4 % compared to 0.2 % concentration nanofluid. The similar findings were reported from an experimental investigation on Al_2O_3 nanofluid by (Yousefi et al. 2012c) where the absorptance of 0.2 wt% nanofluid is higher than 0.4 wt% in lower temperature difference, but lower in higher temperature differences. This phenomenon had been explained by some investigators (i.e., Zhou and Ni 2008; Vatanpour et al. 2011). However, higher temperature increased the speed of molecules and collisions between the nanoparticles that increased the thermal conductivity for higher concentration nanofluid (Das and Choi 2009).

Exergy analysis

Figure 7 shows the exergy efficiency of various flow rates with different working fluid types for the flat-plate solar collector experiment. Based on the efficiency Eqs. (10) and (13) as well as efficiency data shown in Fig. 6, increasing mass flow rate will increase the exergy efficiency of the system. Adding more SiO_2 nanoparticles to the system, from 0.2 to 0.4 %, can produce higher exergy efficiency than the water. The uncertainty for collector exergy efficiency calculation at various tests was around 8.5 %. The results indicate that in solar collector, there is a definite probability to get maximum exergy using SiO_2 nanofluid as medium. The possible reason for this enhancement may be

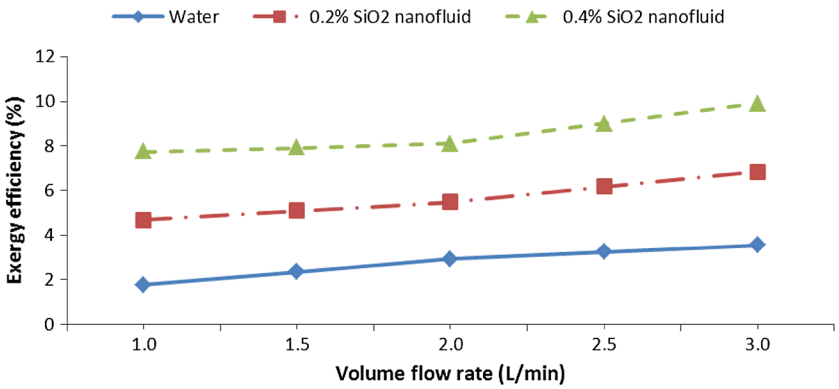

Fig. 7 Effect of volume flow rate of working fluid on the exergy efficiency of the solar collector

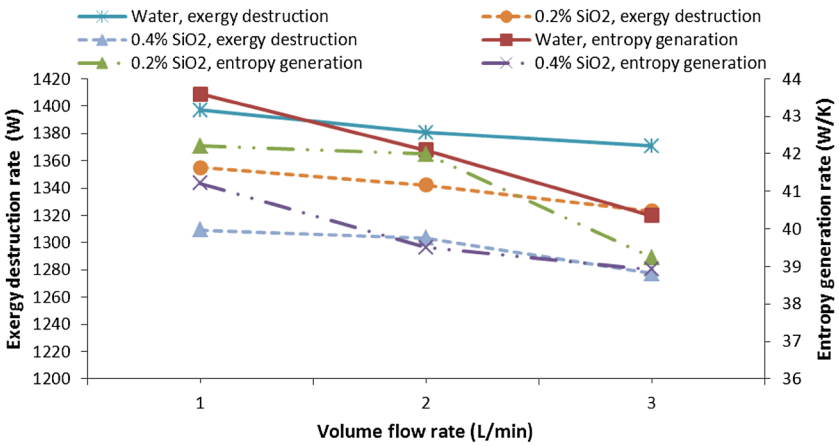

Fig. 8 Effect of volume flow rate of working fluid on the exergy destruction and entropy generation of the solar collector

associated with the increase in thermal conductivity of the mixture and higher convective heat transfer coefficient of nanofluid. The results complied with those obtained from Duangthongsuk and Wongwises (2009) and He et al. (2007).

Exergy destruction and entropy generation

The exergy destruction and entropy generation rates are presented in Fig. 8. As shown in the figure, the rates decreased by increasing the volume flow rates for all types of the working fluids. Exergy is the maximum output potential that can be achieved by a system relative to the dead state or environment temperature. Exergy efficiency implied how close the performance of the system had achieved relative to its theoretical limit. Exergy destruction, however, is the cause of a system not achieving its maximum capabilities and it can be avoided. This exergy destruction, if minimized and managed further, can increase the energy and exergy efficiency of the system even more. Adding nanoparticles in the base fluid can be seen to lower down the entropy generation and exergy destruction. Thermal conductivity and heat absorption rates increase with the increment of nanoparticles volume fraction and thus result in reduction of entropy generation and exergy destruction. Although adding nanoparticles in the fluid will increase the viscosity and fluid friction that will lead to increase of the entropy generation in the system, entropy generation will decrease far greater than fluid friction due to the gap of contribution of heat transfer. Similar result was reported by Mahian et al. (2012).

Heat transfer and fluid flow

Figure 9 illustrates the effect of SiO_2 nanoparticles concentration on the heat transfer coefficient. The uncertainty for collector heat transfer coefficient calculation at various tests was around 4.9 %.

Enhanced heat transfer coefficient is observed by adding SiO_2 nanoparticles in the base fluid due to the improvement of thermal conductivity of nanofluids (Table 1). Thermal conductivity is normally proportional to the heat transfer coefficient. Jiang et al. (2014) indicated that for an identical Nusselt number condition, heat transfer coefficient of a fluid is higher when the thermal conductivity of the fluid becomes higher. At higher particle volume fraction, higher convective heat transfer coefficient was observed. Suspension of thermal boundary layer formation and

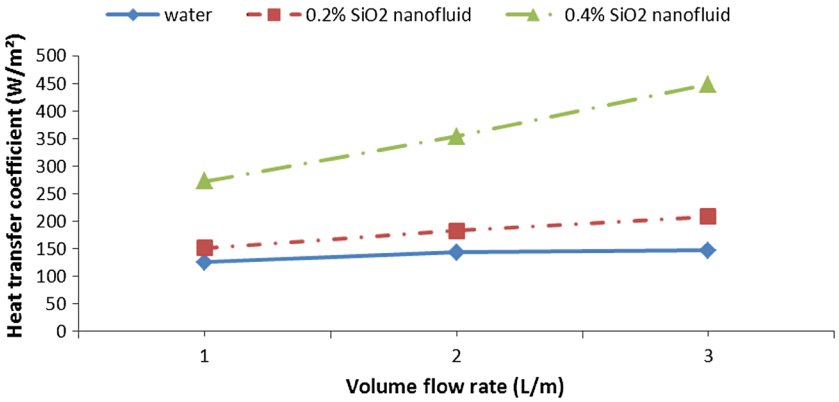

Fig. 9 Effect of volume flow rates of working fluids on the heat transfer coefficient of the solar collector

Table 5 Specific heat, density, and Prandtl number of the working fluids

	Specific heat, C_p (J/kg K)	Density, ρ (kg/m^3)	Prandtl number, *Pr*
Water	4,182	1,000	5.576
0.2 % SiO_2 nanofluid	4,113.66	1,059.4	4.825
0.4 % SiO_2 nanofluid	4,045.32	1,118.8	3.7934

disturbance of the SiO_2 nanoparticles in the mixture could also rise at higher concentration of nanofluid and, therefore, resulting in higher heat transfer coefficient. Results are agreed with Kabeel et al. (2013) and Khairul et al. (2014).

Table 5 shows the value of the specific heat, the density, and the Prandtl number of the working fluid calculated from Eqs. (14), (34), and (45), respectively. Adding SiO_2 nanoparticles to the water has increased the density of the fluid while decreasing the specific heat and the Prandtl number. A decrease in the specific heat has led to smaller amount of the heat energy needed to raise the temperature that will lead to higher output temperature when applied in the solar collector. Decreasing the Prandtl number has resulted in bigger thickness of the thermal boundary layer than the velocity boundary layer.

The measured viscosity of nanofluids in this study is shown in Fig. 10. It is shown in Fig. 10 that the viscosity of nanofluid exponentially decreases with the increase of temperature, and the viscosity value of the nanofluid is higher than the base fluid for every addition of volume concentration.

The Reynolds number is a dimensionless value of the ratio of inertial force to viscous force in fluid flow. Figure 11 indicates that the Reynolds number increased by increasing the volume flow rate of the working fluid and by adding SiO_2 nanoparticles, and the value of the Reynolds number can be enhanced further. The maximum uncertainty calculated for Reynolds number was around 1.1 %.

For a forced convection flow, the Nusselt number is a very important parameter because it deals with the heat transfer at the boundary layer of fluid. The Nusselt number is a dimensionless ratio of convective to the conductive heat transfer normal to the boundary, while it is a function of the Reynolds and Prandtl numbers. As seen in Fig. 12, the Nusselt number increased by adding nanoparticles inside the working fluid and thus managed to improve the

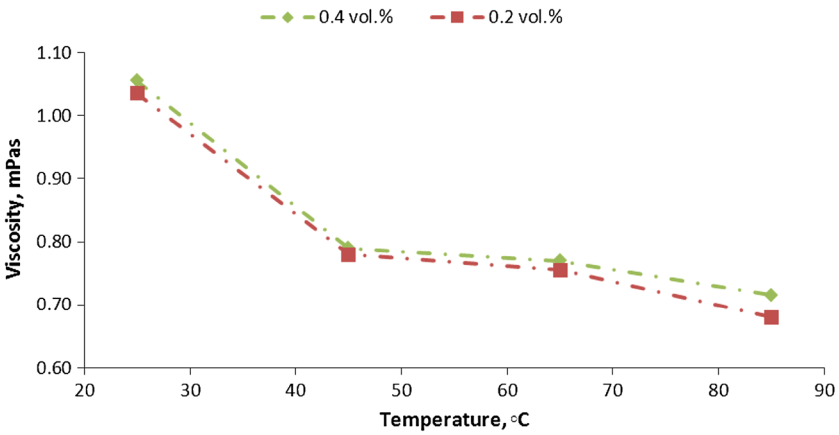

Fig. 10 Measured value of viscosity for nanofluids in this study

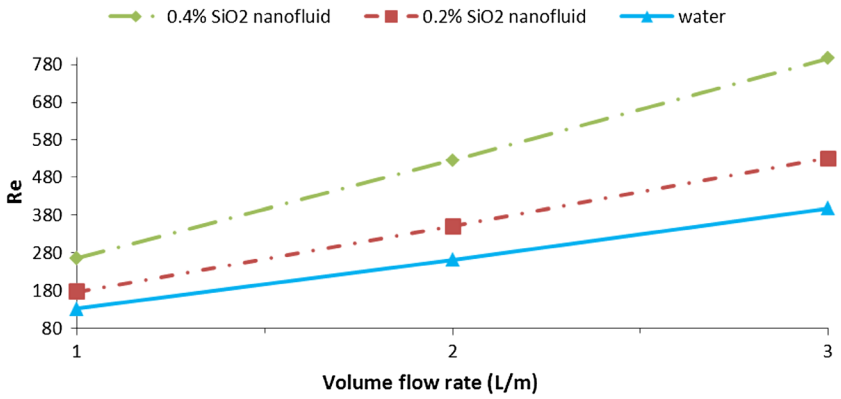

Fig. 11 Effect of volume flow rate on Reynolds numbers

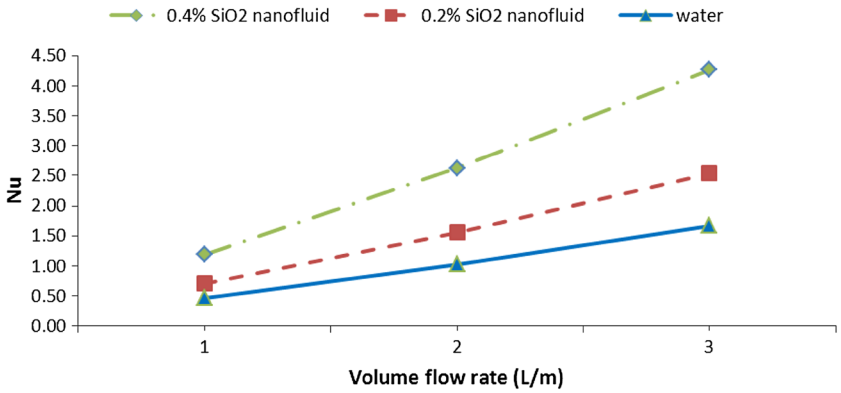

Fig. 12 Effect of volume flow rate on Nusselt numbers

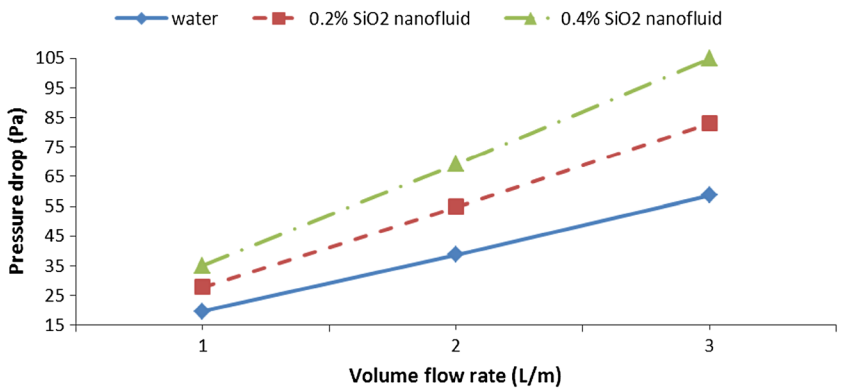

Fig. 13 Effect of volume flow rate of working fluid on the pressure drop

heat transfer characteristic in the system for the corresponding Reynolds number, as reported by other researchers (Azmi et al. 2013a, b).

Pumping power

Suspending solid particles to enhance the heat transfer and efficiency in fluids had been tested many times before using millimeter or micrometer-sized particles but were not very practical due to problems such as increased pressure drop of the flow channel, and thus increasing the pumping power needed by the system. However, the production of nanometer-sized particles brings little or no penalty in pressure drop and pumping power because the nanoparticles are ultrafine. In this section, the results in pressure drop and pumping power of using nanofluids in solar collectors are shown and discussed.

Figure 13 shows that the pressures drop in the system as a function of volume flow rate for different types of working fluids. The pressure drop increased by increasing the working fluid flow rate and by adding the nanoparticles concentration. The higher pressure drop experiences using nanofluid because of its higher density, as explained by Tiwari et al. (2013).

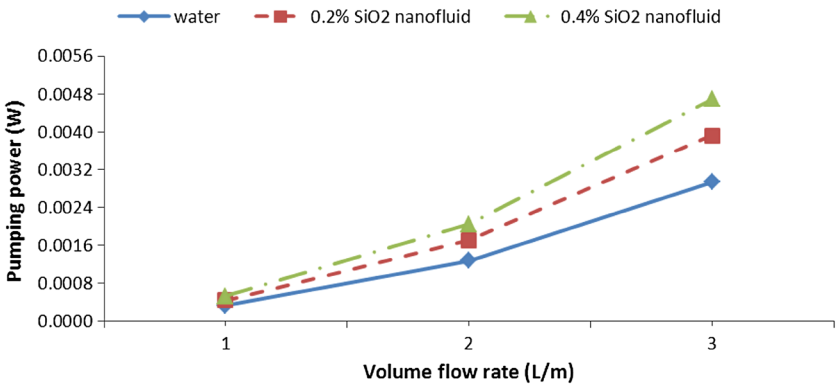

Fig. 14 Effect of volume flow rate of working fluid on the pumping power

Table 6 Embodied energy and percentage of energy savings to manufacture solar thermal collector when using different nanofluids

	Water	SiO_2 nanofluid (calculated from experimental result)	SiO_2 nanofluid (in comparison with theoretical result from Faizal et al. 2013a)
Embodied energy (MJ)	1,064.7	785.50	928.00
Energy saving (%)		26.22	21.56

Table 7 Economic comparison of solar collectors with different types of fluids

	Electric heater	Solar heater (water)	Solar heater (SiO_2) in this study	Solar heater (SiO_2) from Faizal et al. (2013a)
Capital costs (USD)	124.73			
Independent costs (USD)		935.45	935.45	935.45
Area based costs (USD)		311.82	227	244.58
Nanoparticles (USD)			23.11	23.11
Total cost (USD)	124.73	1,247.27	1,185.56	1,203.14
Electricity cost saving per year (USD)		500.78	500.78	500.78
Years until electricity savings = costs		2.49	2.37	2.40

Figure 14 demonstrates the effect of nanofluid on the pumping power for varying nanoparticle concentrations with different volume flow rates. As shown in the figure, the pumping power needed for the SiO_2 nanofluid is slightly higher compared to the water, and it increases by increasing of the nanoparticles volume fraction. The pumping power is associated with the mass flow rates, the density, and the pressure drop of the working fluids, as expressed in Eq. (38). Adding more nanoparticles to the working fluid will result in increasing of the density and the pressure drop, and thus increasing the pumping power for the system. The similar results had also been reported by some investigators (Kabeel et al. 2013; Khairul et al. 2014). However, the penalty in pressure drop and pumping power using nanofluid is so small in which it does not give any significant impact on the effective efficiency of the system.

Energy savings

Table 6 presents the embodied energy for each collector as well as the percentage of energy savings when applying the SiO_2 nanofluid in the solar collector compared to the water as the working fluid. As seen in Table 5, the reduction in the copper and the glass material in the nanofluid-based solar collector results in a reduction of around 280 MJ when compared to the water-based collector. The similar results had also been shown by Otanicar (2009) for graphite nanofluids' direct absorption solar collector and from analytical results by Faizal et al. (2013a).

Cost savings

The size reduction of nanofluid-based solar collector can lead to electricity cost savings calculated based on the current prices for electricity in Malaysia, as shown in Table 7. Daily energy load for an electric heater is estimated to be around 11 kWh. Due to the higher efficiency of the nanofluid-based solar collector, the yearly cost savings for SiO_2 nanofluids are greater than that of the water-based solar collector.

The payback period for the SiO_2 nanofluid collector is less than that of the conventional collector primarily due to

Table 8 Embodied energy emissions from various working fluid solar collectors

	Solar heater (water)	Solar heater (SiO_2) in this study	Solar heater (SiO_2) from Faizal et al. (2013a)
Embodied energy (MJ)	1,064.7	785.5	928
Emission (kg)			
Carbon dioxide, CO_2	646.27	476.80	563.30
Sulfur oxides, SO_x	0.33	0.24	0.29
Nitrogen oxides, NO_x	0.56	0.42	0.49

Table 9 Yearly damage costs for various working fluid solar collectors

	Cost (USD/kg)	Damage costs (USD)		
		Solar heater (water)	Solar heater (SiO_2) in this study	Solar heater (SiO_2) from Faizal et al. (2013a)
Carbon dioxide, CO_2	0.03	17.76	13.11	15.49
Sulfur oxides, SO_x	11.24	3.71	2.74	3.23
Nitrogen oxides, NO_x	17.05	9.62	7.10	8.39
Total (USD)		31.10	22.94	27.11

the reduced capital cost of the collector. The SiO_2 nanoparticles can be considered one of the cheapest nanoparticles available in the market due to its abundance. Further savings with nanofluid-based solar collectors can be achieved if the price of nanoparticles is expected to drop as they become more widely used and produced.

Emissions and damage cost reduction

As seen in Table 8, the manufacturing of the SiO_2 nanofluids-based solar collector results in around 170 kg less CO_2 emissions compared to a conventional solar collector. The differences between the other emissions, sulfur oxides (SO_x), and nitrogen oxides (NO_x) are of a much smaller scale. Finally, the offset damage costs from the pollution savings of the collectors are established in the next section.

Table 9 shows that the damage cost is lower with the nanofluid-based solar collector. These costs savings are not directly applicable to the collector owner, but distributed throughout the installer of the collector, the utility, or the state and federal government. This damage costs indicate the impact of the pollutants from the manufacturing of the collector, but the economic or environmental impacts of nanoparticles are not included. Studies have been done on the impact of nanoparticles on the environment, especially human health and ecological systems (Chen et al. 2008), but they focused on nanoparticles which were not suspended in liquid. For the nanofluid solar collector, the SiO_2 nanoparticles are dispersed in water, which can eliminate the risk for inhalation and it runs on a closed loop cycle.

Conclusions

The analysis and performance assessment of a flat-plate solar thermal collector using SiO_2 nanofluid as absorbing medium has dealt from energetic, exergetic, economic, and environmental aspects in this study. An experimental investigation has also been conducted, and the relevant relations are used in which the analyses have presented. Nanofluids containing small amount of nanoparticles have higher energy and exergy efficiency than base fluids. The efficiency of solar collector increased by 23.5 % using 0.2 % SiO_2 nanofluid. In term of heat transfer, addition of a small amount of SiO_2 nanoparticles has resulted in the increased Nusselt and Reynolds number. As a result, the heat transfer characteristic in the system has enhanced. The negative impact of adding nanoparticles in the base fluids is the increase in viscosity of the working fluid that has led to increase in pumping power and pressure drop. However, for low concentration nanofluids, only negligible effect in the pumping power and pressure drop is noticed. Due to higher efficiency of the solar collector operated by nanofluid, smaller and more compact solar collector could be manufactured that can reduce the energy and cost to manufacture it. The reduction in the copper and the glass material in the nanofluid-based solar collector results in a reduction of around 280 MJ when compared to the water-based collector. Therefore, it would result in lower emission and lower impact on the environment compared to a conventional collector. The manufacturing of the SiO_2 nanofluids-based solar collector results in around 170 kg less CO_2 emissions compared to a conventional solar collector.

Acknowledgments The authors would like to acknowledge the financial support provided by the University of Malaya under UMRG Project no.: RP015B-13AET and Ministry of Education Malaysia for UM-MoE High Impact Research Grant (HIRG) scheme (Project no.: UM.C/HIR/MoHE/ENG/40).

References

Alim MA, Abdin Z, Saidur R, Hepbasli A, Khairul MA, Rahim NA (2013) Analyses of entropy generation and pressure drop for a conventional flat plate solar collector using different types of metal oxide nanofluids. Energy Build 66:289–296

Ardante F, Beccali G, Cellura M, Brano VL (2005) Life cycle assessment of a solar thermal collector. Renew Energy 30:1031–1054

ASHRAE (2010) Methods of testing to determine the thermal performance of solar collectors (ANSI approved). Atlanta, USA

Azmi WH, Sharma KV, Sarma PK, Mamat R, Anuar S, Dharma Rao V (2013) Experimental determination of turbulent forced convection heat transfer and friction factor with SiO_2 nanofluid. Exp Therm Fluid Sci 51:103–111

Bejan A (1996) Entropy generation minimization: the method of thermodynamic optimization of finite-size systems and finite-time processes, vol 2. CRC Press, Boca Raton

Bejan A, Keary DW, Kreith F (1981) Second law analysis and synthesis of solar collector systems. J Sol Energy Eng 103:23–28

Bergman TL, Lavine AS, Incropera FP, DeWitt DP (2011) Fundamentals of heat and mass transfer, 7th edn. Wiley, Hoboken

Cengel YA, Boles MA (2010) Thermodynamics: an engineering approach, 7th edn. McGrawHill, New York

Chen Z, Meng H, Xing G, Guan H, Zhao F, Liu R, Chang X, Gau X, Wang T, Jia G, Ye C, Chai Z, Zhao Y (2008) Age-related differences in pulmonary and cardiovascular response to SiO_2 nanoparticles inhalation: nanotoxicity has susceptible population. Environ Sci Technol 42:8985–8992

Chen Y-j , Wang P-y, Liu Z-h (2013) Application of water-based SiO_2 functionalized nanofluid in a loop thermosyphon. Int J Heat Mass Transf 56:59–68

Choi SUS (1995) Enhancing therm conductivity of fluids with nanoparticles. ASME FED 231:99–103

Das SK, Choi SUS (2009) A review of heat transfer in nanofluids. In: Irvine TF, Hartnett JP (eds) Advances in heat transfer. Elsevier, New York, pp 81–197

de Sanchez-Bautista AF, Santibanez-Aguilar JE, Ponce-Ortega JM, Napoles-Rivera F, Serna-Gonzalez M, El-Halwagi MM (2014) Optimal design of domestic water-heating solar systems. Clean Technol Environ Policy. doi:10.1007/s10098-014-0818-4

Duangthongsuk W, Wongwises S (2009) Heat transfer enhancement and pressure drop characteristics of TiO_2–water nanofluid in a double-tube counter flow heat exchanger. Int J Heat Mass Transf 52:2059–2067

Esen H (2008) Experimental energy and exergy analysis of double-flow solar air heater having different obstacles on absorber plates. Build Environ 43:1046–1054

Faizal M, Saidur R, Mekhilef S, Alim MA (2013) Energy, economic and environmental analysis of metal oxides nanofluid for flat-plate solar collector. Energy Convers Manag 76:162–168

Faizal M, Saidur R, Mekhilef S (2013b) Potential of size reduction of flat-plate solar collectors when applying MWCNT nanofluid. Earth Environ Sci 16:1–4

Faizal M, Saidur R, Mekhilef S (2014) Potential of size reduction of flat-plate solar collectors when applying Al_2O_3 nanofluid. Adv Mater Res 832:149–153

Farahat S, Sarhaddi F, Ajam H (2009) Exergetic optimization of flat plate solar collectors. Renew Energy 34:1169–1174

Foster R, Witcher J, Nelson V, Ghassemi M, Mimbela LE, Ghassemi A (2009) Sol energy: renewable energy and the environment. Taylor and Francis, New York

Garg HP, Agarwal RK (1995) Some aspects of a PV/T collector/forced circulation flat plate solar water heater with solar cells. Energy Convers Manag 36:87–99

Gupta KKD, Saha SK (1990) Energy analysis of solar thermal collectors. Renew Energy Environ 1:283–287

He Y, Jin Y, Chen H, Ding Y, Cang D, Lu H (2007) Heat transfer and flow behaviour of aqueous suspensions of TiO_2 nanoparticles (nanofluids) flowing upward through a vertical pipe. Int J Heat Mass Transf 50:2272–2281

Ise N, Sogami I (2005) Structure formation in solution: ionic polymers and colloidal particles. Springer, Berlin

Jiang H, Li H, Zan C, Wang F, Yang Q, Shi L (2014) Temperature dependence of the stability and thermal conductivity of an oil-based nanofluid. Thermochim Acta 579:27–30

Kabeel AE, Abou El Maaty T, El Samadony Y (2013) The effect of using nano-particles on corrugated plate heat exchanger performance. Appl Therm Eng 52:221–229

Kahani M, Heris SZ, Mousavi SM (2013) Effects of curvature ratio and coil pitch spacing on heat transfer performance of Al_2O_3/water nanofluid laminar flow through helical coils. J Dispers Sci Technol 34:1704–1712

Kalogirou S (2004) Environmental benefits of domestic solar energy systems. Energy Convers Manag 45:3075–3092

Kalogirou S (2008) Thermal performance, economic and environmental life cycle analysis of thermosyphon solar water heaters. J Sol Energy 83:39–48

Kalogirou S (2009) Solar energy engineering: processes and systems. Academic Press, Burlington

Kamyar A, Saidur R, Hasanuzzaman M (2012) Application of computational fluid dynamics (CFD) for nanofluids. Int J Heat Mass Transf 55:4104–4115

Khairul MA, Alim MA, Mahbubul IM, Saidur R, Hepbasli A, Hossain A (2014) Heat transfer performance and exergy analyses of a corrugated plate heat exchanger using metal oxide nanofluids. Int Commun Heat Mass Transf 50:8–14

Kline SJ, McClintock FA (1953) Describing uncertainties in single-sample experiments. Mech Eng 75:3–8

Kosmulski M (2001) Chemical properties of material surfaces. Marcel Dekker, New York

Kotas TJ (1995) The exergy method of thermal plant analysis. Krieger Publish Company, Malabar

Kotulski ZA, Szczepinski W (2010) Error analysis with applications in engineering. Springer, Dordrecht

Kulkarni DP, Das DK, Vajjha RS (2009) Application of nanofluids in heating buildings and reducing pollution. Appl Energy 86:2566–2573

Lalchand G (2012) Electricity demand and supply in Peninsular Malaysia: energy efficiency, renewable energy, or nuclear? http://www.christopherteh.com/. Accessed 21 Dec 2012

Lenert A, Wang EN (2012) Optimization of nanofluid volumetric receivers for solar thermal energy conversion. Sol Energy 86:253–265

Leong KY, Saidur R, Kazi SN, Mamun AH (2010) Performance investigation of an automotive car radiator operated with nanofluid-based coolants. Appl Therm Eng 30:2685–2692

Leong KY, Saidur R, Mahlia TMI, Yau YH (2012) Predicting size reduction of shell and tube heat recovery exchanger operated with nanofluids based coolants and its associated energy saving. Energy Educ Sci Technol A 30:1–14

Li Q, Xuan Y, Wang J (2003) Investigation on convective heat transfer and flow features of nanofluids. J Heat Transf 125:151–155

Li FC, Yang JC, Zhou WW, He YR, Huang YM, Jiang BC (2013) Equation experimental study on the characteristics of thermal conductivity and shear viscosity of viscoelastic-fluid-based nanofluids containing multiwalled carbon nanotubes. Thermochim Acta 556:47–53

Liu Z-h, Liao L (2008) Sorption and agglutination phenomenon of nanofluids on a plain heating surface during pool boiling. Int J Heat Mass Transf 51:2593–2602

Lu L, Liu Z-H, Xiao H-S (2011) Thermal performance of an open thermosyphon using nanofluids for high-temperature evacuated tubular solar collectors: Part 1: indoor experiment. Sol Energy 85:379–387

Mahian O, Mahmud S, Heris SZ (2012) Analysis of entropy generation between co-rotating cylinders using nanofluids. Energy 44:438–446

Mahian O, Kianifar A, Kleinstreuer C, Al-Nimr MdA, Pop I, Sahin AZ, Wongwises S (2013) A review of entropy generation in nanofluid flow. Int J Heat Mass Transf 65:514–532

Mekhilef S, Safari A, Mustaffa WES, Saidur R, Omar R, Younis MAA (2012) Solar energy in Malaysia: current state and prospects. Renew Sustain Energy Rev 16:386–396

Namburu P, Kulkarni D, Dandekar A, Das D (2007) Experimental investigation of viscosity and specific heat of silicon dioxide nanofluids. Micro Nano Lett IET 2:67–71

Nemet A, Kravanja Z, Klemeš JJ (2012) Integration of solar thermal energy into processes with heat demand. Clean Technol Environ Policy 14:453–463

Otanicar TP (2009). Direct absorption solar thermal collectors utilizing liquid-nanoparticle suspensions. Arizona State University

Otanicar T, Phelan PE, Prasher RS, Rosengarten G, Taylor RA (2010) Nanofluid-based direct absorption solar collector. J Renew Sustain Energy 2:033102

Owhaib W, Palm B (2004) Experimental investigation of single-phase convective heat transfer in circular microchannels. Exp Therm Fluid Sci 2:105–110

Ranjan KR, Kaushik SC (2013) Exergy analysis of the active solar distillation systems integrated with solar ponds. Clean Technol Environ Policy 16:791–805

Saidur R, Lai YK (2011) Nanotechnology in vehicle's weight reduction and associated energy savings. Energy Educ Sci Technol A 26:87–101

Saidur R, BoroumandJazi G, Mekhilef S, Jameel M (2012) Exergy analysis of solar energy applications. Renew Sustain Energy Rev 16:350–356

Shin D, Banerjee D (2011) Enhancement of specific heat capacity of high-temperature silica-nanofluids synthesized in alkali chloride salt eutectics for solar thermal-energy storage applications. Int J Heat Mass Transf 54:1064–1070

Singal RK (2008) Non-conventional energy resources (alternative energy sources and systems). S.K. Kataria and Sons, Delhi

Spardo JV, Rabl A (1999) Estimates of real damage from air pollution: site dependence and simple impact indices for LCA. Int J LCA 4:229–243

Sustainable Energy Development (2010) Ninth Malaysia plan

Suzuki A (1988) General theory of exergy balance analysis and application to solar collectors. Energy 13:153–160

Taylor RA, Phelan PE, Otanicar TP, Adrian R, Prasher R (2011) Nanofluid optical property characterization: towards efficient direct absorption solar collectors. Nanoscale Res Lett 6:225

Tiwari AK, Ghosh P, Sarkar J (2013) Heat transfer and pressure drop characteristics of CeO_2/water nanofluid in plate heat exchanger. Appl Therm Eng 57:24–32

Tora EA, El-Halwagi MM (2009) Optimal design and integration of solar systems and fossil fuels for sustainable and stable power outlet. Clean Technol Environ Policy 11:401–407

Tsillingiridis G, Martinopoulos G, Kyriakis N (2004) Life cycle environmental impact of a thermosyphon domestic solar hot water system in comparison with electrical and gas water heating. Renew Energy 29:1277–1288

Vatanpour V, Madaeni SS, Moradian R, Zinadini S, Astinchap B (2011) Fabrication and characterization of novel antifouling nanofiltration membrane prepared from oxidized multiwalled carbon nanotube/polyethersulfone nanocomposite. J Membr Sci 375:284–294

Wang H (2009) Dispersing carbon nanotubes using surfactants. Curr Opin Colloid Interface Sci 14:364–371

White FM (2003) Fluid mechanics, 5th edn. McGraw-Hill, Boston

Yang X, Liu Z-h (2010) A kind of nanofluid consisting of surface-functionalized nanoparticles. Nanoscale Res Lett 5:1324–1328

Yousefi T, Shojaeizadeh E, Veysi F, Zinadini S (2012a) An experimental investigation on the effect of pH variation of MWCNT–H_2O nanofluid on the efficiency of a flat-plate solar collector. Sol Energy 86:771–779

Yousefi T, Veisy F, Shojaeizadeh E, Zinadini S (2012b) An experimental investigation on the effect of MWCNT–H_2O nanofluid on the efficiency of flat-plate solar collectors. Exp Therm Fluid Sci 39:207–212

Yousefi T, Veysi F, Shojaeizadeh E, Zinadini S (2012c) An experimental investigation on the effect of Al_2O_3–H_2O nanofluid on the efficiency of flat-plate solar collectors. Renew Energy 39:293–298

Zamzamian A, KeyanpourRad M, KianiNeyestani M, Jamal-Abad MT (2014) An experimental study on the effect of Cu-synthesized/EG nanofluid on the efficiency of flat-plate solar collectors. Renew Energy 71:658–664

Zhou SQ, Ni R (2008) Measurement of the specific heat capacity of water-based Al_2O_3 nanofluid. Appl Phys Lett 92:1–3